Available online at www.sciencedirect.com

SCIENCE DIRECT®

Earth and Planetary Science Letters 226 (2004) 347–366

EPSL

www.elsevier.com/locate/epsl

Origin of enriched ocean ridge basalts and implications for mantle dynamics

Kathleen E. Donnelly[a,*], Steven L. Goldstein[a], Charles H. Langmuir[b], Marc Spiegelman[a]

[a]*Lamont-Doherty Earth Observatory and Department of Earth and Environmental Sciences, Columbia University, 61 Rt. 9W, Palisades, NY 10964, United States*

[b]*Department of Earth and Planetary Sciences, Harvard University, 20 Oxford St., Cambridge, MA 02138, United States*

Received 6 November 2003; received in revised form 15 March 2004; accepted 20 July 2004
Available online 11 September 2004
Editor: B. Wood

Abstract

The Mid-Atlantic Ridge (MAR) south of the Kane Fracture Zone at ~23°N (the MARK area) is distant from hot spots and a type area for "normal" mid-ocean ridge basalt (N-MORB) depleted in highly incompatible elements. High-density sampling reveals that a small proportion of basalt are enriched in incompatible elements (enriched mid-ocean ridge basalts, E-MORB) from the MARK area. It is apparent that enriched magma sources, not associated with hot spots, are widespread in the upper mantle and are a common occurrence on both fast- and slow-spreading ridges.

Evaluation of the trace-element systematics shows that E-MORB generation requires two stages. Low-degree melts metasomatise the upper mantle to create an enriched source, which later undergoes large extents of melting. A significant time lapse between the two events is required by differences in radiogenic isotope ratios. Atlantic, Pacific, and Indian ocean ridges that are far from hot spots show "mantle isochron" ages of ~300 Ma for the Sm–Nd, Rb–Sr, and ^{238}U–^{206}Pb systems after corrections for melting, but these ages need not be indicative of a specific event. Instead, they can result from continuous processes of formation and destruction of enriched mantle sources by melting and convective mixing. A two-box model describing these processes illuminates relationships between mantle isochron ages and upper mantle dynamics. If formation–destruction of enriched mantle is at steady state, constant "mantle isochron" ages are maintained and depend on the residence time of enriched mantle sources, the half-life of the radioactive system, and the daughter element behavior during mantle melting. The common ages of the Sr, Nd, and Pb systems reflects their long half-lives and similar melting behavior. In contrast, $^{207}Pb/^{204}Pb$–$^{206}Pb/^{204}Pb$ ages are approximately twice as old due to the short half-life of ^{235}U relative to the age of the Earth. For the long-lived systems, the mantle isochron ages approximate the residence time of the enriched reservoir, if its mass is a few percent of the system.

We propose that the first stage of melting occurs at depth in subduction zones where the mantle wedge is enriched by the addition of low-degree melts of subducted crust. The second stage of greater extents of melting occurs beneath ocean ridges.

* Corresponding author. Tel.: +1 845 365 8660; fax: +1 845 365 8155.
E-mail address: donnelly@ldeo.columbia.edu (K.E. Donnelly).

0012-821X/$ - see front matter
doi:10.1016/j.epsl.2004.07.019

The model results suggest that the mantle is currently in quasi-steady state and that the size of the system (N-MORB plus E-MORB sources) is similar to the upper mantle. The time scale of ~300 Ma for survival of E-MORB sources indicates rapid convective stirring and efficient reprocessing of the upper mantle by plate tectonics.

Keywords: E-MORB; upper mantle; mantle evolution; isotope geochemistry; trace-element geochemistry; mid-ocean ridge basalt; mantle isochron; convective mixing

1. Introduction

The earliest studies of ocean ridge basalts (MORB) recognized that segments near hot spots display enrichments in highly incompatible elements. The origin of "enriched mid-ocean ridge basalts" (E-MORB) has been explained by interaction of enriched plumes from the deep mantle with the depleted upper mantle source of "normal mid-ocean ridge basalts" (N-MORB) (e.g., Refs. [1,2]). The origin of E-MORB far from hot spots is more controversial. Hanson [3] first suggested that enriched basalts reflect preferential melting of veins in the mantle. E-MORB have been sporadically sampled both on- and off-axis at the East Pacific Rise (EPR) [4–10]. Their origin has been attributed to small plumes dispersed as small-scale heterogeneities at fast spreading ridges [11] and to melting of enriched eclogitic veins derived from subducted oceanic crust recycled into the upper mantle [7,12–15]. In both models, enriched sources are related to recycling of subducted oceanic crust, following the suggestions of Hofmann and White [16] and Allègre and Turcotte [17]. Other sources of enrichment include fractionation during melting or metasomatic events [18,19].

We report here the discovery of E-MORB on the Mid-Atlantic Ridge (MAR) south of the Kane transform fault (the MARK area), a region regarded as a type locality for N-MORB [20–23] and show that the E-MORB source influences the chemistry of several of the more "normal" ridge basalts from the segment. The MARK area is far from any hot spot, and the E-MORB is chemically similar to those found on other ridges. The spreading rate of Atlantic ridges is much slower than in the Pacific, and plumes are less likely to be dispersed by fast mantle convection. It thus appears that enriched MORB may occur without any clear relationship to plumes in all ocean basins [24–26]. This calls for a reevaluation of E-MORB origin separate from injection of deep plumes into the upper mantle. Taking into account trace-element and radiogenic isotope systematics of N- and E-MORB, we evaluate implications for average ages of upper mantle heterogeneity and rates of formation and destruction of E-MORB sources.

2. Discovery of E-MORB in the MARK area

Seventy rock cores were collected along 10 transects of the MARK area on R/V *Atlantis II*, cruise AII129-7. Several of the shallowest samples are enriched in incompatible elements (Fig. 1a and Table 1) with Th, Ba, Rb, and Nb abundances more than an order of magnitude higher than N-MORB and H_2O higher by a factor of 4 (J. Dixon, personal communication). In contrast, major-element differences between enriched and depleted basalts are subtle. E-MORB have slightly higher alumina and sodium and lower silicon and iron. The E-MORB source influences less than 5% of the recovered lavas at MARK (Fig. 2). The trace-element enrichment reflects a long-term source enrichment because the E-MORB have higher Sr and Pb and lower Nd isotope ratios, which correlate with incompatible element abundances.

3. Constraints on the origin of E-MORB

An important aspect of the E-MORB geochemical signature is the large fractionations among highly incompatible elements. For example, Ba/La ratios are a factor of ~5 higher than N-MORB, whereas moderately incompatible element ratios such as Sm/

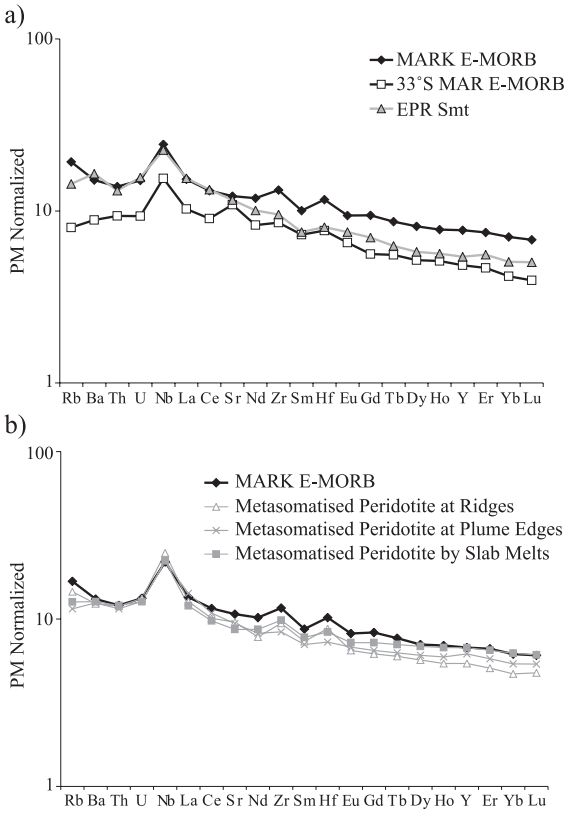

Fig. 1. Enriched MORB from the MARK area. (a) Trace-element pattern of the MARK E-MORB compared to other E-MORB. MARK E-MORB is enriched in highly incompatible elements and similar to E-MORB erupted on off-axis Pacific seamounts [10] and the southern MAR [24]. (b) The E-MORB trace-element signature requires a first stage of low-degree (low-F) partial melting that metasomatises the mantle, which is later subjected to higher degree (high-F) melting. Three scenarios of low-F melt metasomatism are shown. The MARK E-MORB trace-element pattern (diamond) can be generated by high-F melting of the metasomatised mantle. For the ridge and plume edge model, the first melt stage is of a garnet lherzolite with 5% garnet in which F=0.5% or 2%. The low-F melts then contribute 6% or 1.5%, respectively, to metasomatised peridotite, which is frozen into the lithosphere, subducts, and later reappears beneath the ridge to partially melt to F=10%, forming E-MORB. For subducted slab melts, the first-stage low-F melt is of a garnet pyroxenite with 20% garnet with F=1%, which metasomatises the overlying mantle wedge and is 0.5% of the mixture. Following recirculation, the metasomatized mantle partially melts beneath a ridge to F=9% to form E-MORB. Starting source compositions and partition coefficients are in Tables 1 and 3. "PM normalized" means normalized to primitive mantle values [58].

La differ by less than a factor of 3 (Fig. 2, Table 2). These differences place important constraints on the origin of E-MORB.

Enriched mantle sources for ocean island basalts (OIB) are often attributed to recycled oceanic crust [16,27]. However, recycled oceanic crust is problematic because oceanic crust generally shows increasing depletion of trace elements with increasing incompatibility, opposite to E-MORB. Because eclogitic recycled ocean crust is likely to melt to large extents, particularly beneath ocean ridges [28], re-melting of recycled crust would not produce the observed relative enrichments (Fig. 2). Re-melting of E-MORB or OIB could produce E-MORB trace-element patterns, but OIB generally have too high Sr and too low Nd isotope ratios to be the source of E-MORB. Subducted sediments are also precluded because of their distinct trace-element and isotopic signatures (e.g., low Ce/Pb, high Ba/Nb, La/Nb, and $^{207}Pb/^{204}Pb$). Fluids addition alone cannot produce E-MORB because neither Th nor La are fluid mobile [29] and will not generate high Th/La (Fig. 2b).

On the other hand, low-degree partial melting, if the extent of melting (F) is of the same order as the bulk partition coefficient (D), can fractionate highly incompatible elements and preserve the mantle isotopic signature. The concentration of an element in a melt (C_l) is related to the source abundance (C_o) by the modal melting equation

$$C_l = C_o/(F + D(1 - F)) \quad (1)$$

Alternatively, non-modal melting can be described by

$$C_l = C_o/(D_o + F(1 - P)) \quad (2)$$

where P corresponds to the bulk partition coefficient in the melt and D_o in the initial solid mode. Elements with D<0.01, such as Ba, Th, and La, require very small extents of melting to achieve the observed fractionations (Fig. 2). Therefore, the E-MORB trace-element signature appears to reflect very low extents of melting.

Formation of E-MORB beneath the ocean ridge by low-degree melting, however, is problematic. Near chondritic heavy rare-earth element (HREE) ratios (e.g., Dy/Yb_N~1, Fig. 3) constrain the presence of residual garnet to less than a few percent. Low-degree melting under ridges takes place deep in the melting regime where garnet is stable and at the edges of the melting envelope. At the extremely low degrees of melting (~0.2%) required for element fractionations such as Th/La, the HREE ratios such

Table 1
Average E-MORB, N-MORB, and source compositions

	MARK E-MORB AII129-7 RC17A	MARK N-MORB AII129-7 RC55	EPR Smt E-MORB R109-005	SEIR E-MORB WW 10-126-7	S&M N-MORB	D	E	Recycled Crust EPR-AVG	OIB
Latitude	23°20.1′ N	23°30.1′ N	14°9.2′ N	49°31.8′ S					
Longitude	44°57.8′ W	44°55.45′ W	104°18.1′ W	109°28.8′ E					
Depth (m)	3700	4060	2610	3240					
SiO_2	49.58	50.56	50.56						
TiO_2	1.68	1.54	1.43						
Al_2O_3	16.42	15.68	15.9						
FeO total	8.98	9.58	8.34						
MgO	7.90	7.81	7.79						
CaO	10.66	11.39	12.1						
Na_2O	3.31	3.1	2.66						
K_2O	0.59	0.12	0.48						
P_2O_5	0.26	0.21	0.23						
Rb	11.58	0.67	8.62	8.39	0.56	0.040	0.684	1.35	0.934
Ba	99.71	6.79	108.6	95.6	6.3	0.540	7.54	14.78	11.22
Th	1.10	0.14	1.044	1.15	0.12	0.007	0.086	0.200	0.124
U	0.305	0.05	0.318	0.289	0.047	0.0033	0.023	0.08	0.035
Nb	16.05	2.39	14.878	13	2.33	0.199	1.33	3.79	2.08
La	9.91	3.47	10.04	9.64	2.5	0.237	0.737	4.36	1.62
Ce	21.99	10.89	22.29		7.5	0.841	1.65	13.4	3.73
Sr	243	133.2	230	243	90	11.4	18.51	123.8	38.9
Pb	0.82	0.47	0.798	0.989	0.3	0.04	0.075	0.590	0.181
Nd	14.81	10.74	12.57	12.8	7.3	0.854	1.23	12.28	2.40
Zr	139	108.62	100		74	8.06	11.2	122.4	16.10
Hf	3.29	2.76	2.281		2.05	0.230	0.288	3.12	0.464
Sm	4.08	3.61	3.19	3.48	2.63	0.338	0.392	4.10	0.677
Eu	1.45	1.32	1.16		1.02	0.137	0.149	1.46	0.282
Gd	5.14	5	3.81		3.68	0.494	0.536	5.67	0.867
Tb	0.858	0.89	0.62		0.67	0.091	0.097	0.990	0.138
Dy	5.48	5.86	3.9		4.55	0.628	0.666	6.56	0.891
Ho	1.16	1.27	0.84		1.01	0.141	0.148	1.42	0.196
Er	3.28	3.56	2.44		2.97	0.423	0.437	4.02	0.641
Y	33.21	35.71	23.3		28	4.10	4.28	40.3	6.04
Yb	3.11	3.37	2.23		3.05	0.427	0.441	3.91	0.587
Lu	0.458	0.52	0.34		0.455	0.065	0.068	0.590	0.091
$^{87}Sr/^{86}Sr$	0.702761	0.702348	0.702719	0.70336					
$^{143}Nd/^{144}Nd$	0.513109	0.513181	0.513111	0.512909					
$^{206}Pb/^{204}Pb$	18.526	18.285	18.496	18.198					
$^{207}Pb/^{204}Pb$	15.536	15.484	15.510	15.512					
$^{208}Pb/^{204}Pb$	38.158	37.706	38.133	38.262					

Compositions of MARK E-MORB, a typical MARK N-MORB, SEIR E-MORB [49], EPR Smts [10,41], and average N-MORB from Sun and McDonough [55]. Analytical methods are discussed in Table 2. Major elements are reported in wt.%, and trace elements are reported in ppm. The source compositions used for the melting curves in Fig. 2 and the two-stage models in Fig. 1b are also given: depleted mantle (D), enriched mantle (E), recycled oceanic crust/garnet pyroxenite (EPR AVG), and ocean island basalt (OIB). Average East Pacific Rise MORB is taken as an approximation of subducted crust. The composition is based on recent ICP-MS trace-element data [59].

as Dy/Yb are too fractionated (Dy/Yb_N~1.8), HREE abundances are far too low (Yb~1.26 ppm) to yield E-MORB (Fig. 3), and the abundances of elements such as Th and Ba are much too high, enriched by a factor of ~500 relative to the source (or $1/D$). Even for more compatible elements like Yb, at 0.2% partial melting, the enrichment in the melt still approaches $1/D$. These abundances would be low-

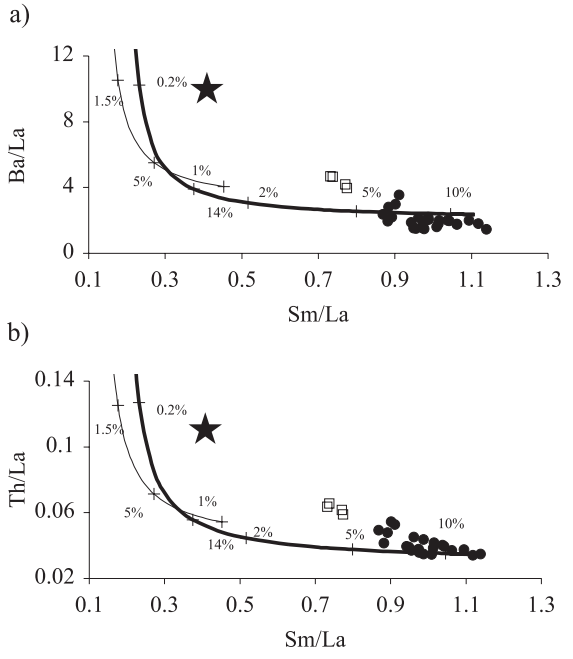

Fig. 2. Trace-element ratios of MORB from the MARK area. (a) Ba/La and Sm/La. (b) Th/La and Sm/La. The MARK E-MORB (star) requires low-degree (low-*F*) partial melting to generate the observed fractionations among highly incompatible elements. Depleted MORB are the circles, and samples influenced by the E-MORB source are the squares. The thick curve represents partial melting of a depleted mantle composition of spinel lherzolite. The extent of melting is denoted on the curve. *F* must be as low as 0.2% to account for the E-MORB trace-element ratios. The thin curve represents partial melting of subducted oceanic crust, garnet pyroxenite. *F* is also denoted and must be as low as 1% even with this more enriched source. The large Th/La fractionation argues against the influence of a fluid, since neither element is fluid mobile. Solid and liquid modes for lherzolite melting: 0.18 cpx, 0.30 opx, 0.52 ol; and 0.75 cpx, −0.10 opx, 0.35 ol, respectively. Solid and liquid modes for the pyroxenite melting: 0.20 gar, 0.80 cpx; and 0.11 gar and 0.89 cpx, respectively. Source compositions are listed in Table 1. In MARK, additional complexities argue for two depleted MORB components (Donnelly et al., in preparation), which does not change the requirements for low-*F* melting to generate the trace-element ratios in E-MORB.

ered if the lherzolite mantle source was extremely depleted in trace elements, but such a scenario is inconsistent with the time-integrated incompatible element enrichment (i.e., high Rb/Sr, U/Pb, and low Sm/Nd), indicated by E-MORB isotope ratios compared to that for N-MORB.

Melting of eclogitic veins also is not consistent with low-degree partial melting beneath ridges. Eclogite begins to melt at greater pressures than peridotite, yielding an eclogite/garnet pyroxenite residue [28]. A low-degree melt would have concentrations too high for many elements and too strongly fractionated HREE (Dy/Yb_N~2.2, Fig. 3). Furthermore, eclogitic veins would enhance the extent of melting because of their low melting temperatures and would result in equal or greater melting extents compared to N-MORB.

The major-element similarities between E-MORB and N-MORB are consistent with similar source mineralogy and extent of melting. Slightly elevated Al_2O_3 and lower FeO can be attributed to higher water and alkali contents during melting and low pressure differentiation and thus do not indicate substantial major-element differences in primary magmas [30–32]. Michael and Chase [30] showed the importance of high H_2O in E-MORB for suppressing plagioclase fractionation, leading to higher Al_2O_3 and lower FeO. While E-MORB characteristically show elevated Al_2O_3, lower FeO is not universal. E-MORB and N-MORB from the MAR at 33°S have similar FeO and Na_2O [24]. Where FeO is lower and alkalis are higher, such as in the MARK area, the lower FeO can result from the higher olivine/liquid partition coefficient caused by increased alkali contents, as well as the effect of water contents on the liquid line of descent [31,33]. Therefore, the subtle major-element differences between E-MORB and N-MORB appear to be related to water and alkali content, and E-MORB major-element compositions do not require significantly lower extents of partial melting.

These various considerations thus predict equal or greater extents of melting for E-MORB mantle compared to the surrounding N-MORB. Since N-MORB from normal ridge depths, such as the MARK area, are well constrained to result from $F \approx 0.1$ [34]; similarly high extents of melting are expected for E-MORB. Even if somehow the extent of melting for E-MORB were lower by a factor of 3, this would not explain the trace-element systematics.

3.1. Two-stage model for E-MORB generation

The apparent paradox that trace-element abundances in E-MORB indicate large extents of partial melting, while trace-element ratios that require low-

Table 2
MARK Data

Sample	Latitude	Longitude	Depth	MgO	$^{87}Sr/^{86}Sr$	$^{143}Nd/^{144}Nd$	Rb	Sr	Nd	Sm	Ba	Th	La
KNO115 TK-25	23.62°N	44.89°W	5100	7.19	0.702373		0.89	132	12.93	4.33	8.52	0.18	4.27
KNO115 TK-11	23.58°N	44.90°W	4770–4830	7.33	0.702428	0.513210	0.43	111	13.03	4.54	7.45		4.27
AII129-7 RC35	23.56°N	44.91°W	4760	7.55			0.68	128	11.56	3.92	6.88	0.15	3.87
AII129-7 RC31	23.56°N	44.91°W	4660	7.07	0.702355		1.06	134	13.21	4.49	10.05	0.21	4.67
AII129-7 RC46	23.53°N	44.92°W	4380	7.13			0.86	132	13.12	4.52	8.68	0.18	4.35
AII129-7 RC47	23.53°N	44.91°W	4380	7.04	0.702411	0.513191	0.75	126	12.30	4.24	7.75	0.15	3.87
AII129-7 RC53	23.50°N	44.95°W	4160	7.01			0.69	134	14.04	4.66	7.46	0.19	4.91
AII129-7 RC64	23.48°N	44.92°W	4140	6.72	0.702428	0.513184	1.37	137	14.74	4.92	12.11	0.26	5.51
AII129-7 RC76	23.44°N	44.94°W	3900	6.92	0.702445	0.513191	1.36	136	13.56	4.47	12.22	0.25	5.15
AII129-7 RC77	23.44°N	44.94°W	3780	7.91	0.702333	0.513198	0.50	125	9.85	3.40	5.43	0.10	3.04
KNO115 TK-14	23.42°N	44.94°W	3610	7.22	0.702378	0.513212	1.44	143	13.03	4.42	14.00		5.00
AII129-7 RC72	23.42°N	44.96°W	4000	7.35			0.93	132	13.08	4.54	9.33	0.20	4.59
AII129-7 RC37	23.39°N	44.94°W	3680	7.35	0.702423	0.513190	0.65	128	11.74	4.04	6.72	0.14	3.81
AII129-7 RC38	23.39°N	44.93°W	3780	7.55			0.71	137	11.92	4.02	7.42	0.16	4.12
AII129-7 RC39	23.38°N	44.93°W	3900	8.47	0.702437	0.513192	0.46	142	9.88	3.30	5.17	0.13	3.46
KNO115 TK-15	23.36°N	44.96°W	3450–3430	7.91	0.702376	0.513182	1.29	134	10.31	3.51	13.63	0.20	3.85
AII129-7 RC23	23.36°N	44.97°W	3860	7.50	0.702600	0.513164	3.10	163	13.69	4.35	27.72	0.38	5.94
AII129-7 RC27	23.36°N	44.94°W	3680	7.48	0.702518	0.513171	2.40	151	12.39	4.04	21.91	0.32	5.24
AII129-7 RC25	23.36°N	44.96°W	3700	8.27			1.26	137	10.19	3.41	11.30	0.21	3.78
AII129-7 RC30	23.36°N	44.93°W	3700	8.05			0.52	137	11.53	3.88	8.62	0.14	3.93
AII129-7 RC19A	23.34°N	44.96°W	3500	7.41	0.702439	0.513156	2.85	166	13.16	4.16	26.17	0.37	5.63
AII129-7 RC19B	23.34°N	44.96°W	3500	7.48			0.77	146	12.21	4.05	8.90	0.19	4.59
AII129-7 RC16	23.34°N	44.97°W	3920	8.54	0.702426	0.513211	0.35	111	8.31	3.02	3.86	0.09	2.65
AII129-7 RC20	23.34°N	44.95°W	3600	7.68	0.702355	0.513190	0.67	130	11.25	3.75	7.45	0.16	3.98
AII129-7 RC18	23.34°N	44.96°W	3600	7.87			2.14	160	12.56	4.07	20.86	0.31	5.25
AII129-7 RC86	23.30°N	44.95°W	3760	7.49	0.702404	0.513199	0.51	135	10.62	3.57	5.69	0.12	3.54
AII129-7 RC88	23.30°N	44.96°W	3740	7.57	0.702351	0.513190	0.64	142	12.67	4.34	6.88	0.17	4.46
AII129-7 RC91	23.30°N	44.98°W	3800	7.78	0.702347	0.513189	0.52	138	11.64	3.93	5.96	0.14	4.02
AII129-7 RC84	23.30°N	44.94°W	3860	6.85			0.68	132	13.57	4.64	7.36	0.18	4.77

Trace elements were measured by ICP-MS at LDEO with typical errors of 3–5%. Concentrations were calculated from calibration curves of measured USGS and "in-house" standards. Sr and Pb isotope ratios were measured at LDEO on a Micromass Sector 54 30 thermal ionization mass spectrometer. $^{87}Sr/^{86}Sr$ ratios were normalized to $^{86}Sr/^{88}Sr=0.1194$, with typical ^{88}Sr beam intensities of 4×10^{-11} amps. Replications of the NBS987 standard during three intervals yielded 0.710198 ± 16, (2σ external reproducibility, $n=44$), 0.710246 ± 14 (2σ, $n=6$), 0.710247 ± 9 (2σ, $n=8$). Measurements during the first interval were by static multicollection; the other two were by dynamic multicollection. $^{143}Nd/^{144}Nd$ ratios were measured as NdO+ and normalized to $^{146}Nd/^{144}Nd=0.7219$, with typical $^{144}Nd^{16}O$ beam intensities of 0.5×10^{-11} amp. Replications of the La Jolla Nd standard averaged $^{143}Nd/^{144}Nd=0.511838\pm9$ (2σ, $n=34$). All samples were further corrected to value of 0.511860 for the La Jolla standard. Pb isotope ratios were measured using a ^{207}Pb–^{204}Pb double spike. Reproducibility is 183, 284, and 300 ppm (2σ, $n=16$) for $^{206}Pb/^{204}Pb$, $^{207}Pb/^{204}Pb$, and $^{208}Pb/^{204}Pb$ ratios, respectively. Measured values are corrected to $^{206}Pb/^{204}Pb=16.9356$, $^{207}Pb/^{204}Pb=15.4891$, and $^{208}Pb/^{204}Pb=36.7006$ [60]. Some samples were measured more than once, and the reproducibility was consistent with the standards. For these, the average value is listed. MgO values were measured on glass chips using the electron microprobe at the American Museum of Natural History. Depths are reported in meters below sea level.

degree melting can be accommodated through creation of E-MORB in two stages. First, low-degree melts are added to normal mantle peridotite sources to generate fractionated ratios of highly incompatible elements. Second, the enriched source is melted to a "normal" extent beneath ocean ridges. The two-stage process leads to the necessary trace-element fractionations and concentrations (e.g., Fig. 1b, Table 3), major-element compositions similar to N-MORB, and isotope ratios that reflect long-term source enrichment.

In which tectonic scenarios might such two-stage processes occur, and what additional constraints can be used to choose among them? Two-stage processes involving low-degree melts have been proposed for formation of continental rift volcanics [35] and continental crust [36]. Low-degree partial melts may occur in different mantle

settings as a consequence of mantle convection and plate circulation. Scenarios for low-degree partial melting that metasomatise the surrounding mantle to generate E-MORB include low-degree melting of peridotite or eclogite in the wings of a ridge melting regime [18,37–42] or in the margins of plumes [43]. We also suggest that low-degree melting of subducting oceanic crust as eclogite at depth, metasomatising the mantle wedge or nearby mantle during subsequent circulation in the mantle convective system, is a potentially powerful source of metasomatism (Fig. 1b). As the isotope ratios require time for radiogenic ingrowth, the subsequent high-degree melting event would have to take place under ocean ridges after plate recirculation. The critical common factor is the need for two stages, one where a low-degree melt produces the trace-element fractionations, and a second where a high-degree melt produces the E-MORB major- and trace-element abundances. Isotope ratios can be used to constrain the timing of the low-degree melt event.

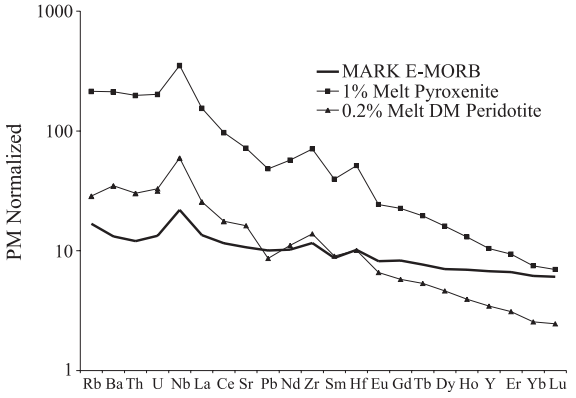

Fig. 3. Trace-element patterns E-MORB and low-degree (low-F) melts. The low-F melts of peridotite and pyroxenite are characterized by steep primitive mantle normalized trace-element patterns, while the E-MORB trace-element patterns are relatively flat and thus are not low-F melts. While the garnet pyroxenite and garnet lherzolite low-F melts have different trace-element abundances, their patterns are similar. This similarity, despite the different source compositions and mineralogy, is in part because the garnet pyroxenite is recycled MORB, whose trace-element pattern is derived from peridotite. Equally important is that at very low F values the melt resembles the bulk Ds. For both mineralogies, garnet and clinopyroxene mainly determine the bulk Ds. Solid and liquid modes for the garnet lherzolite: 0.05 gar, 0.27 cpx, 0.12 opx, 0.56 ol; and 0.25 gar, 0.53 cpx, 0.14 opx, 0.08 ol, respectively. Modes for the garnet pyroxenite are reported in Fig. 2. "PM normalized" means normalized to primitive mantle values [58].

Table 3
Partition coefficients used

	Garnet	Clinopyroxene	Orthopyroxene	Olivine
Lu	4.5	0.439	0.052	0.02
Yb	4.18	0.432	0.047	0.017
Er	3.2	0.422	0.041	0.0087
Y	2.8	0.421	0.025	0.007
Ho	2.0	0.41	0.029	0.006
Tb	1.0	0.382	0.021	0.002
Gd	0.8	0.37	0.016	0.00099
Dy	1.4	0.402	0.025	0.004
Eu	0.5	0.355	0.013	0.00015
Hf	0.115	0.23	0.013	0.005
Sm	0.115	0.28	0.01	0.0006
Zr	0.27	0.128	0.013	0.0013
Nd	0.06	0.19	0.007	0.0002
Sr	0.003	0.096	0.009	0.008
Ce	0.007	0.09	0.003	0.00006
La	0.001	0.042	0.0005	0.00005
Nb	0.0042	0.007	0.0001	0.000041
U	0.027	0.0052	0.00005	0.00005
Th	0.0015	0.003	0.00005	0.00005
Rb	0.00001	0.0006	0.00045	0.000045
Ba	0.00001	0.00068	0.00004	0.000043

The K_d values are based on experimental data when available. Otherwise, the K_d is estimated using best knowledge of how different elements behave relative to those elements, which do have experimentally determined K_d. Several references were used to choose the clinopyroxene (Cpx) [61–65] and garnet (Gt) K_d values [61,65–67]. The absolute value of the K_d chosen may not correspond to the absolute values reported in the literature, but the relative relationship among elements reflects the relative differences measured experimentally [61,62,66–69]. The K_d values for orthopyroxene are based on Hanson [69] and Kennedy et al. [68], and the K_d values for olivine are based on Kennedy et al. [68].

4. Mantle isochrons and their significance

The concept of "mantle isochrons" was developed in the 1960s and 1970s in classic papers dealing principally with the systematics of ocean island basalts (e.g., Refs. [44–46]). These studies suggested that positive correlations observed on isochron diagrams carry age significance. Since then, however, the isotopic variability in oceanic basalts has generally been interpreted to simply reflect mixing of different and unrelated mantle sources without clear age significance. If an isochron has age significance, then the ages shown by multiple radioactive decay systems

must be consistent with one another. This is unlikely to occur through mixing of different mantle sources. For example, mixing among the Zindler–Hart mantle end-member components [12] would not produce the same "age" for different isotope systems on isochron diagrams.

Previous studies have found correlations between parent–daughter and isotope ratios for Rb–Sr, Sm–Nd and U–Th–Pb in erupted basalts of the North Atlantic [47,48], the Southeast Indian Ridge (SEIR) [49], and EPR seamounts [9,39,41,50] (Figs. 4 and 5). The "apparent ages" of some 10^8 years clearly do not reflect the recent melting to form E-MORB at the ridge. The "ages" are younger for Rb–Sr and U–Th–Pb than Sm–Nd. However, correcting for parent–daughter fractionation during melting, using Eq. (2), brings them into agreement (Fig. 7), in which case they may reflect the timing of the first-stage low-degree melting event. The melting corrections steepen the Rb–Sr slope and flatten the Sm–Nd slope, reflecting the relative parent and daughter bulk D values and making the ages older and younger, respectively (Fig. 7). For F=0.1, the correction has a larger effect on the Rb–Sr slope than Sm–Nd because Rb is much more incompatible than Sr, whose bulk D value is similar to Sm and Nd.

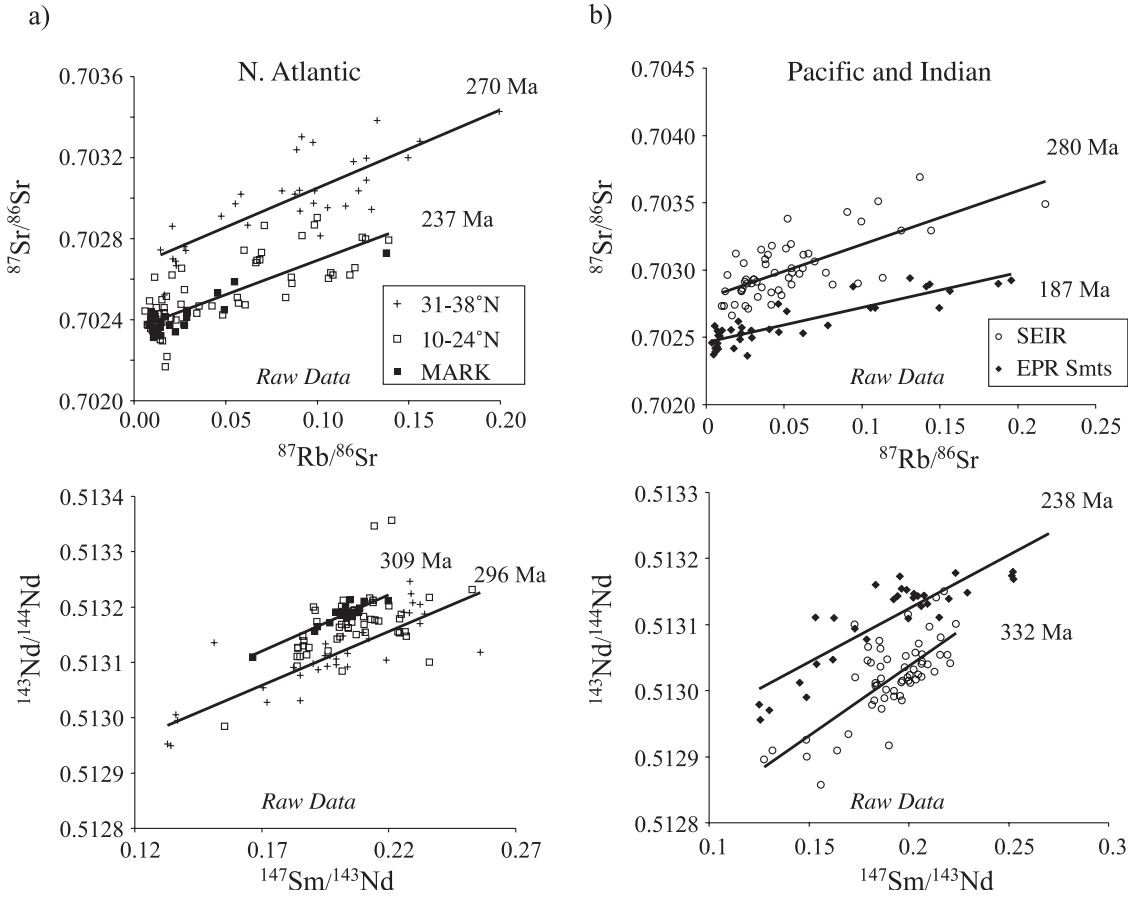

Fig. 4. MORB parent/daughter and isotope ratios. Parent/daughter ratios correlate with isotope ratios of zero-age basalts in regions where E-MORB occur. Regions where there are sufficient data from three different ocean basins show similar systematics: the "ages" of the Sm–Nd correlations are older than the "ages" of the Rb–Sr correlations. The slopes correspond to ages of 200–300 Ma. (a) North Atlantic samples lie on two trends. Those from 31° to 38°N have higher $^{87}Sr/^{86}Sr$ (crosses) than those from 10° to 24°N (open squares) [25,48] New data (this study) from MARK overlap with the data from 10° to 24°N. (b) East Pacific Rise (EPR) Seamounts [10,41] and the Southeast Indian Ridge (SEIR) [49] are offset but show similar correlations.

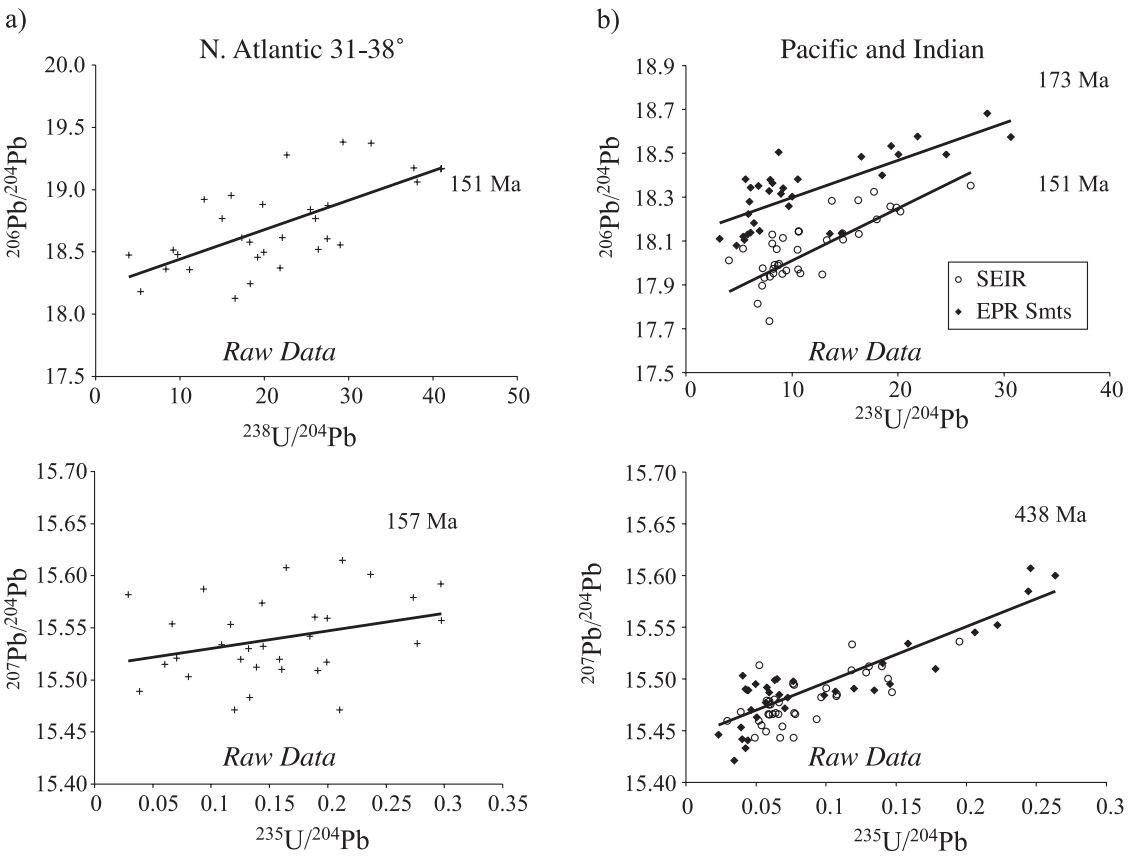

Fig. 5. U–Pb systematics. Samples are those in Fig. 4. (a) "Ages" implied by the ^{238}U–^{206}Pb and ^{235}U–^{207}Pb slopes are younger than for Rb–Sr for the North Atlantic 31–38°N [48]. (b) "Ages" implied by ^{238}U–^{206}Pb slopes of Southeast Indian Ridge (SEIR) basalts [49] are also younger than for Rb–Sr (Fig. 4b). In contrast, the EPR Seamounts [10,41] yield a similar ^{238}U–^{206}Pb "age" to Rb–Sr (Fig. 4b). The ^{235}U–^{207}Pb "ages" for both the SEIR and the EPR Seamounts are much older (~438 Ma). Variable amounts of sulphide in the most recent melting event beneath the ridge will affect U–Pb fractionation and be reflected in the parent/daughter ratios. Remnants of ancient U/Pb fractionation events could lead to ancient ^{207}Pb–^{206}Pb "ages."

The extent of melting to generate the corrected "mantle isochrons" is not chosen arbitrarily, as only certain values yield congruent ages for different isotope systems (Fig. 6). The difference between Sm–Nd and Rb–Sr ages (Δage) is minimized for all ocean basins at F~10–14% (Fig. 6) and increases at smaller and larger F values. U–Th–Pb corrections are more difficult because of the possible effect of variable amounts of sulphide on the bulk D of Pb [48,51,52]. If the amount of sulphide in the upper mantle source results in D_{Pb} similar to Ce or Nd (cf. Ref. [51]), then the slope correction for melting would be similar to for Rb–Sr. We note that EPR seamounts have similar ^{238}U–^{206}Pb (173 Ma) and ^{87}Rb–^{87}Sr "ages" (187 Ma), while ^{238}U–^{206}Pb "age" is much younger than ^{87}Rb–^{87}Sr "age" for the North Atlantic and SEIR (Figs. 4, 5). Given the uncertainty of D_{Pb}, we will focus on Rb–Sr and Sm–Nd in order to compare different ocean basins.

The "mantle isochron" ages for Atlantic, Pacific, and Indian sites are remarkably similar. The age for the MARK area of ~280 Ma when F~10% (Fig. 7a) is similar to the ~250-Ma age of Dosso et al. [48] for the greater North Atlantic, despite an offset in the Rb–Sr arrays for 31–38°N and 10–24°N. The SEIR yields concordant ages of ~306 Ma (Fig. 8b; Ref. [49]). The EPR seamounts yield a slightly younger age of ~220 Ma (Fig. 7c). All of these regions thus show similar average "mantle isochron" ages for both Rb–Sr and Sm–Nd in the range of ~300 Ma.

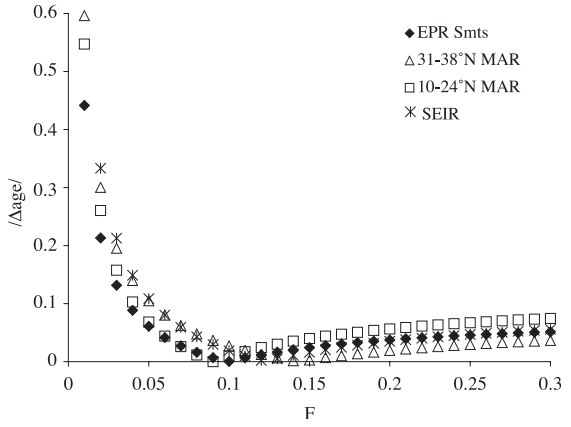

Fig. 6. /Δage/ minima. After MORB correcting parent/daughter ratios for melting using the non-modal batch melting equation (Eq. (2), text) and K_d values (Table 3), mantle isochron ages can be calculated. For variable degrees of melting (F), the mantle isochron age for Rb–Sr can be compared to the Sm–Nd age. Most F-values produce incongruent mantle isochron ages for multiple isotope systems. /Δage/ is the difference between the Rb–Sr and Sm–Nd mantle isochron ages, respectively. The F-value for which /Δage/ is minimized is taken to represent the average melting extent for a given area. All three ocean basins yield similar average F of ~11%. The 31–38°N MAR has slightly higher average F of ~14%, consistent with higher mantle temperatures associated with proximity to the Azores.

In summary, parent–daughter and isotope ratios correlate for young basalts of major ocean basins. Regionally associated basalts, after correcting for reasonable extents of melting under ridges, show similar "mantle isochron ages" of a few hundred million years. As these "ages" are controlled by the presence of E-MORB with enriched parent–daughter and isotope ratios, they may provide constraints on the origin and timing of E-MORB source enrichment.

4.1. A two-box model for steady-state generation of mantle isochrons

The observation that the common radioactive decay systems yield the same "mantle isochron ages" for Atlantic, Pacific, and Indian MORB could be taken as prima facie evidence that they record a discrete upper mantle-wide fractionation event. For example, previous workers have argued that such ages reflect the opening of ocean basins or the break up of Pangea [48,49]. However, since low-degree melt metasomatism as described above is a natural result of plate tectonics, the coupled trace-element and isotopic variations could also reflect continuous creation of chemical heterogeneities by melting, followed by destruction by mantle convection and subsequent melting. For example, previous studies have shown that inferred of "mantle isochrons" [53] or "mantle–crust isochrons" [54] may reflect reservoir mixing times.

We investigate whether the ~300-Ma mantle isochrons can be generated by a repetitive process of low-degree melt metasomatism followed by mantle mixing and a second stage of melting. We use a simple two-box model to approximate the creation of enriched and depleted sources feeding ocean ridges. Low-degree melts form in association with spreading ridges, plumes and other intraplate melting, and subduction zones. They rarely reach the surface and instead metasomatically enrich a part of the mantle. The enriched mantle is convectively remixed into depleted mantle. Thus, new heterogeneities are created by melting and fractionation and gradually destroyed by mixing.

These processes can be represented simply with a box (e) representing metasomatised mantle, the E-MORB source, and another (d) representing the incompatible element-depleted mantle, the N-MORB source (Fig. 8a). A fraction of mantle enriched by low-degree melts is transferred from the depleted to the enriched box, with an equal mass of enriched mantle returned, unfractionated, to the depleted box. The degree of enrichment of an element in e relative to d is described by an "enrichment factor" (α). Appendix A presents a detailed derivation and analytic solution for the behavior of parent–daughter nuclides in this model and is available online from EPSL.

Fig. 7. Corrected mantle isochrons. After the parent/daughter ratios are corrected for melting, Rb–Sr and Sm–Nd mantle isochrons show congruent "ages" (heavy lines). The F-values are calculated using the non-modal batch melting equation (Eq. (2)) as described in the text and Fig. 6. (a) For 10–24°N Atlantic data, including the MARK area, when F=10%, the "ages" are ~280 Ma. (b) For the SEIR data, when F=14%, the "ages" agree at 307 Ma. (c) For the EPR Seamounts, when F=9%, the "ages" agree at 220 Ma. The data show scatter, but reference isochrons bracket the data (dashed lines) and show that the all reasonable "ages" are much less than 500 Ma.

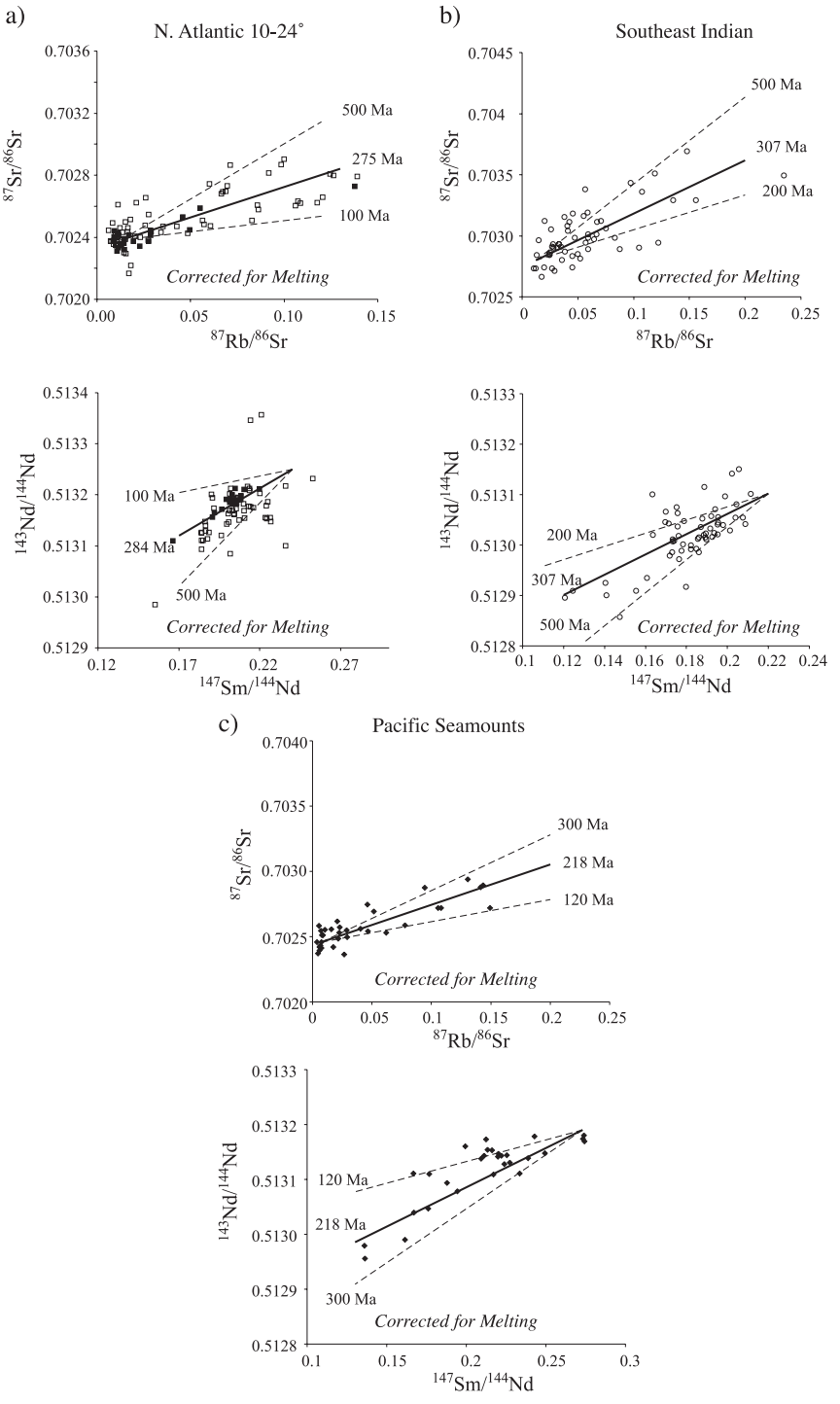
a)
N. Atlantic 10-24°
500 Ma
275 Ma
100 Ma
Corrected for Melting
$^{87}Sr/^{86}Sr$
$^{87}Rb/^{86}Sr$
100 Ma
284 Ma
500 Ma
Corrected for Melting
$^{143}Nd/^{144}Nd$
$^{147}Sm/^{144}Nd$
b)
Southeast Indian
500 Ma
307 Ma
200 Ma
Corrected for Melting
200 Ma
307 Ma
500 Ma
Corrected for Melting
c)
Pacific Seamounts
300 Ma
218 Ma
120 Ma
Corrected for Melting
120 Ma
218 Ma
300 Ma
Corrected for Melting

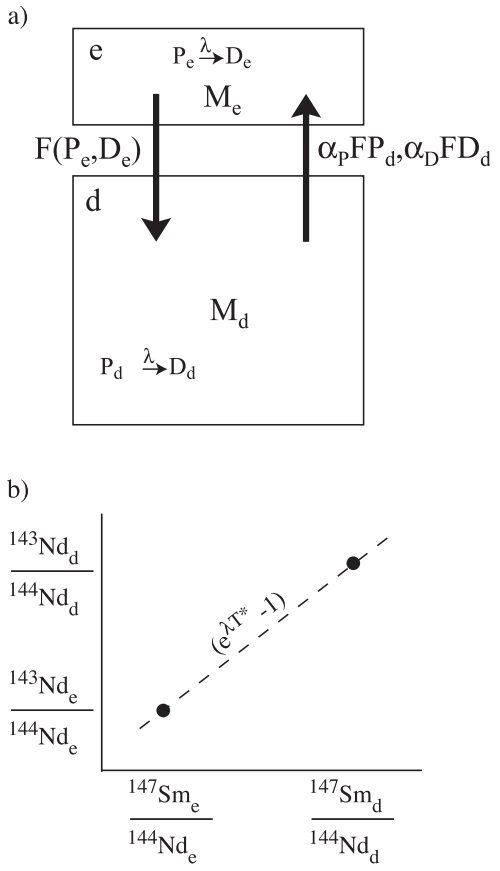

Fig. 8. Two-box model. (a) Cartoon of the two-box model where M_e is the enriched reservoir and M_d is the depleted reservoir. The flux out of M_d is fractionated by the factor α_i for every element i where P_d and D_d represent abundance of the parent (P) and daughter (D) in the depleted reservoir. The flux out of M_e is unfractionated where P_e and D_e represent the abundance of the parent (P) and daughter (D) in the enriched reservoir. The mass fluxes (F) out of the boxes are equal, and therefore, the size of the reservoirs do not change. (b) At any time, the composition of each box can be calculated. From the slope of a mixing line between the two box compositions is the mantle isochron age.

A principal feature of the model is that, for any initial condition, it will evolve to a quasi-steady state of secular equilibrium after an initial transient mixing period, characterized by the mean residence times of the parent and daughter nuclides (see below). In secular equilibrium, the concentration of the parent nuclide in the enriched box will be α_P times that of the depleted box, while the concentration of a stable daughter will be enriched by a factor α_D. These results are physically sensible as in steady state, the flux of a nuclide into and out of either box must be equal. For example, equality of fluxes for the parent implies

$$\alpha_P P_d \, \dot{m} = P_e \dot{m}, \tag{3a}$$

where P_d and P_e are the concentrations by weight of the parent nuclide in the depleted and enriched boxes, respectively. α_P is the enrichment factor for the parent and $\dot{m}$ is the total mass flux between the two boxes. The mass flux equals the amount of metasomatised mantle created, not the amount of low-degree melt, because the model needs to produce E-MORB by ~10% melting of the enriched box. Therefore, in secular equilibrium $P_e/P_d=\alpha_P$. Likewise, for a stable daughter element $D_e/D_d=\alpha_D$. Though the model in the Appendix A tracks the nuclides, in most cases, α_P and α_D approximate the ratio of the elements in the two boxes. If the E-MORB source (Table 1) is formed through low-degree melt metasomatism, then α_D is similar for Nd, Sr, and Pb (1.4–1.8) because they behave similarly during mantle melting. For more incompatible elements such as Rb and Ba, α is higher (~10–20). The α values are dictated by trace-

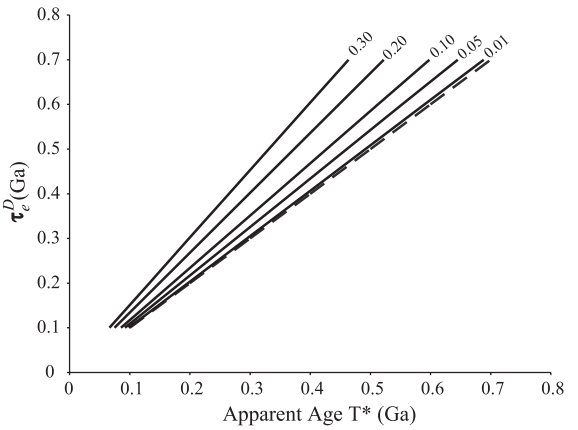

Fig. 9. Apparent age and daughter element residence time of the enriched box. In the model, the mantle isochron age (T^*) is a function of τ_e^D, α_D, and the ratios of the masses of the two boxes (see Eq. (10)). For Rb–Sr, Sm–Nd, U–Pb, α_D~1.7. As shown in the text, when M_e/M_d is small (manifested at ocean ridges by small amounts of E-MORB), then $T^* \sim \tau_e^D$, that is, the mantle isochron age approximates the daughter element residence time in the enriched reservoir. The dashed line represents $M_e=0$.The solid lines are where $M_e>0$ and the value of M_e/M_d is denoted by the number next to each line.

element abundances in E-MORB relative to N-MORB (Table 1). Representative N-MORB from the MARK area (Table 1) is similar to the estimate of Sun and McDonough [55], and therefore, either composition can be used to calculate α. Alternatively, α can be calculated by comparison of modeled N-MORB and E-MORB sources (Table 1). Both methods yield similar values for α.

Given these concentrations and fluxes in secular equilibrium, the following relationships exist between mass residence times and element residence times for both daughter and parent elements in the enriched box:

$$\tau_e = \tau_e^P = \tau_e^D = \frac{M_e}{\dot{m}} \tag{4a}$$

and in the depleted box

$$\tau_d^P = \frac{M_d}{\alpha_P \dot{m}}, \quad \tau_d^D = \frac{M_d}{\alpha_D \dot{m}}, \quad \tau_d = \frac{M_d}{\dot{m}}, \tag{4b}$$

and therefore,

$$\frac{\tau_e}{\tau_d} = \frac{M_e}{M_d}, \quad \frac{\tau_e^D}{\tau_d^D} = \frac{\alpha_D M_e}{M_d}, \quad \frac{\tau_e^P}{\tau_d^P} = \frac{\alpha_P M_e}{M_d}, \tag{4c}$$

where M_e and M_d are the masses; τ_e, τ_d are the mass residence times; and τ_i^P, τ_i^D are the element residence times for the parents and daughters of the enriched and depleted boxes, respectively. Because the element fluxes out of the enriched box are unfractionated, the element residence times are equal to the mass residence time of the enriched box, while for the depleted box, the element residence time depends partly on the incompatibility. The survival time of the enriched box relative to the depleted box simply equals the ratio of their masses. In addition, Appendix A shows that it is useful to define the "mean residence times" for parent and daughter elements in the two-box system as

$$\bar{\tau}^P = \left(\frac{1}{\tau_e^P} + \frac{1}{\tau_d^P}\right)^{-1}, \quad \bar{\tau}^D = \left(\frac{1}{\tau_e^D} + \frac{1}{\tau_d^D}\right)^{-1}, \tag{5}$$

which are the harmonic means of the box residence times (similar to resistors in parallel) and are weighted toward the shorter of the two residence times. For example, if the daughter spends much less time in the enriched box than the depleted box ($\tau_e^D \ll \tau_d^D$), then $\bar{\tau}^D \approx \tau_e^D = (M_e/\dot{m})$; and the mean residence time for the daughter is just its residence time in the enriched box (which happens to be independent of the fractionation factors).

Finally, Appendix A shows that if the concentrations of the enriched and depleted boxes are plotted on an isochron diagram (e.g., Fig. A.2), then in secular equilibrium, they will form a straight line with a slope (s):

$$s = \frac{\lambda \bar{\tau}^D}{1 + \lambda \bar{\tau}^D}. \tag{6}$$

The slope does not change with time, although the isotope ratios increase with time due to radioactive decay. The slope depends only on the decay constant λ and the mean residence time of the daughter element. The parent element fractionation affects the difference in the isotope ratios of the e and d boxes, but not the slope. If this slope is interpreted as a "mantle isochron" with age significance, (i.e., $s = e^{\lambda T^*} - 1$) then an "apparent age", T^*, can be calculated as

$$T^* = -\frac{1}{\lambda} \ln\left(1 - \lambda \bar{\tau}^D\right). \tag{7}$$

If the residence time is much shorter than the decay time (i.e., $\lambda \bar{\tau}^D \ll 1$), Eq. (7) simplifies to

$$T^* \approx \bar{\tau}^D, \tag{8}$$

and the apparent age is simply the mean residence time of the daughter element. If, in addition, the enriched box has a significantly smaller mass than the depleted box, then $T^* \approx \tau_e^D = (M_e/\dot{m})$, which depends only on the mass of the enriched box and the total mass flux (and is independent of any fractionation factors).

Eq. (8) is a valid approximation for long half-life radioactive systems in which daughter ingrowth is nearly linear, for example, if $\bar{\tau}^D$=300 Ma, then $T^* \approx$ 300 Ma, which is the same as the result for long-lived isotopes if the complete equation (Eq. (7)) was used: T^*=301 and 300 Ma for Rb–Sr and Sm–Nd, respectively. For decay systems where the ingrowth rate decreases significantly over geologic

time, the approximation $\lambda\bar{\tau}^{D} \ll 1$ might not be valid, and Eq. (7) must be used. For ^{238}U–^{206}Pb and ^{235}U–^{207}Pb, Eq. (7) yields T^*=307 and 356 Ma, respectively. T^* is thus underestimated by only 2% for ^{238}U–^{206}Pb, but 19% for ^{235}U–^{207}Pb. Therefore, among the relevant decay systems in the Earth, the only one where λ is sufficiently large to require Eq. (7) is ^{235}U–^{207}Pb.

The older ^{235}U–^{207}Pb isochron ages propagate into older $^{206}Pb/^{204}Pb$–$^{207}Pb/^{204}Pb$ (Pb–Pb) ages. From the Pb isotopes of the *e* and *d* boxes, the "apparent Pb–Pb age" (T^*_{Pb-Pb}) can be calculated from the slope on a $^{206}Pb/^{204}Pb$–$^{207}Pb/^{204}Pb$ diagram. This Pb–Pb age is related to the "apparent parent–daughter ages" on conventional isochron diagrams for ^{238}U–^{206}Pb (T^*_{206}) and ^{235}U–^{207}Pb (T^*_{207}) by:

$$S_{Pb-Pb} = \frac{^{235}U\left(e^{\lambda_{235}T^*_{207}} - 1\right)}{^{238}U\left(e^{\lambda_{238}T^*_{206}} - 1\right)} = \frac{^{235}U\left(e^{\lambda_{235}T^*_{Pb-Pb}} - 1\right)}{^{238}U\left(e^{\lambda_{238}T^*_{Pb-Pb}} - 1\right)}, \quad (9)$$

where S_{Pb-Pb} is the slope on a $^{206}Pb/^{204}Pb$–$^{207}Pb/^{204}Pb$ diagram and T^*_{Pb-Pb} is the apparent Pb–Pb age. For the case above where τsuper D=300 Ma and T^*_{Nd}~300 Ma, T^*_{Pb-Pb}=684 Ma. Therefore, older ^{207}Pb–^{206}Pb ages are predicted by the two-box model as a consequence of the shorter ^{235}U half-life. This is an important distinction from the situation where an isochron dates an event, in which case all of the decay systems, irrespective of the half-life, will give the same age.

Note that T^* does not strictly correspond to any event but reflects the parent–daughter and isotopic divergence that is maintained between the boxes. At ocean ridges, mixtures of magmas from E-MORB and N-MORB sources would lie along the isochron line (Fig. 8b). In this context, the "mantle isochron" reflects a continual process where two end-member reservoirs are created and remixed together and thus differs from an isochron reflecting a single age event (cf. Refs. [53,56]). If the ~300-Ma ages of MORB represent a single event, the ages represented by the mantle isochrons would increase with time. If, instead, the age reflects quasi-steady-state creation and destruction of enriched mantle, then the age of the mantle isochron will remain constant and reflects the rates of mixing of the two reservoirs.

4.1.1. How are isochron ages related to reservoir characteristics?

Combining Eqs. (4), (5), and (8) yields an expression for the isochron age in terms of residence times, masses, and the daughter element fractionation:

$$T^* = \tau_e^D \left(\frac{1}{1 + \left(\alpha_D M_e / M_d\right)} \right) \quad (10)$$

The age will only differ significantly from τ_e^D if $(\alpha_D M_e/M_d)$ is significantly greater than zero. For Sr, Nd, and Pb, where $\alpha_D \approx 1.7$, the only way that the apparent age would differ significantly from the residence time in the enriched box is if the enriched box is comparable in size to the depleted box (Fig. 9). In a case where the enrichment factor is much greater than a factor of 2, the apparent age may differ significantly from τ_e^D. For T^*=300 Ma and M_e/M_d=0.03 (similar to the fraction of E-MORB found in MARK), when α_D=2 then τ_e^D=318 Ma. τ_e^D increases to 345 Ma when α_D=5 and to 390 Ma when α_D=10. For Sr, Nd, and Pb, however, α_D<2, and the important variable controlling the relationship between T^* and τ_e^D becomes M_e/M_d, or the size of the smaller, enriched reservoir.

The time interval required for the system to reach secular equilibrium is also of interest. Appendix A shows that differences in concentrations from secular equilibrium decay exponentially due to mixing, with decay times equal to the mean residence times ($\bar{\tau}^D$,$\bar{\tau}^P$). Thus, if $\bar{\tau}^D \approx \bar{\tau}^P \approx 300$ Ma, then any initial transient should vanish by four to five decay times or 1.2–1.5 Ga (See Fig. A.1 for an example).

These results are similar in some respects to the conclusions of Allègre and Lewin [53], although their approach is different. They use a single-box model for the evolution of isotope and trace-element variability in the mantle. They create heterogeneity with a forcing term that drives an increase in variability with time. Their model also goes to steady state where reduction in variability due to mixing and decay balance the forcing term. In steady state, the "apparent age" (T^*) is the residence time within the single box, which would be the similar to our depleted box. In contrast, for the model presented here, we show that the apparent age is the mean residence time of the daughter element

$\tau^{D} \approx \tau^{D}_{e}$, which will tend to be the residence time in the enriched box. In addition, here, we model the concentrations of elements in the two boxes through time and not simply the variability in isotope compositions. The forcing term in Allègre and Lewin is more related to the introduction of heterogeneity through subduction and not directly related to trace-element enrichment of E-MORB. Our model is distinguished by including two reservoirs, a specific geological process of low-degree melting to cause the fractionation between the reservoirs and a match between MORB data and the model. Nevertheless, many characteristics and results of the models, including a Pb–Pb age that is about twice the Rb–Sr and Sm–Nd ages, are similar because all simple chemical box models have similar behavior in terms of decaying eigenmodes (Appendix A). Christensen and Hofmann [57] also found older Pb–Pb ages than the mean differentiation ages of reservoirs in their numerical models.

5. Discussion

Although the two-box model is a gross simplification of mantle processes, it reproduces some key chemical and isotopic aspects of MORB. Using reasonable α values for E-MORB and N-MORB mantle sources and assuming that the E-MORB source forms in two stages as discussed above, the two-stage model is able to generate both end members of the "mantle isochron" array as steady-state compositions for the depleted and enriched reservoirs. Geographically separated ocean basins would be expected to show similar but not necessarily identical mantle isochron ages. The similar ages for the Sr, Nd, and ^{238}U–^{206}Pb decay systems are a consequence of the similar melting behavior of the daughter elements and the small size of the enriched reservoir.

The model follows the conclusions of Allègre and Lewin [53] in that it accounts to some extent for the older Pb–Pb ages as compared to the younger parent–daughter isochron ages. As explained above, faster ^{235}U–^{207}Pb decay causes its "conventional isochron" age to be older than ^{238}U–^{206}Pb, and as a result, the Pb–Pb age derived from the coupled decay of ^{235}U and ^{238}U is also older. The predicted Pb–Pb age of ~700 Ma when T^* for ^{238}U–^{206}Pb is ~300 Ma is consistent with Pb isotope ratios of basalts from 31° to 38°N in the North Atlantic (Fig. 10). The SEIR also yields a similar Pb–Pb age of 815 Ma [49]. However, the model does not explain all Pb isotope data. For the EPR Seamounts, the Pb–Pb age of 2.15 Ga is an order of magnitude older than the conventional isochron ages. If the Pb–Pb age reflected a discrete event that since has evolved as a closed system, the ^{238}U–^{206}Pb and ^{235}U–^{207}Pb conventional isochron ages would also be 2.15 Ga. The fact that the conventional isochron arrays are so different from 2.15 Ga demonstrates the importance of recent U–Pb fractionation. Early Earth U/Pb fractionations, before ^{235}U effectively decayed away, are driving these old Pb–Pb "ages", while recent low-F melt metasomatic events are driving the younger ages for ^{238}U–^{206}Pb and ^{235}U–^{207}Pb, similar to Rb–Sr and Sm–Nd systems.

5.1. Implications for sizes of mantle reservoirs

Chemical and isotopic considerations thus indicate that low-degree melting and metasomatism are important factors contributing to the composition of the upper mantle. Here, we consider the further implications in terms of reservoir sizes and how they may relate to mantle dynamics.

Fig. 11 shows the relationship between mantle isochron ages for Sr, Nd, and Pb isotopes and

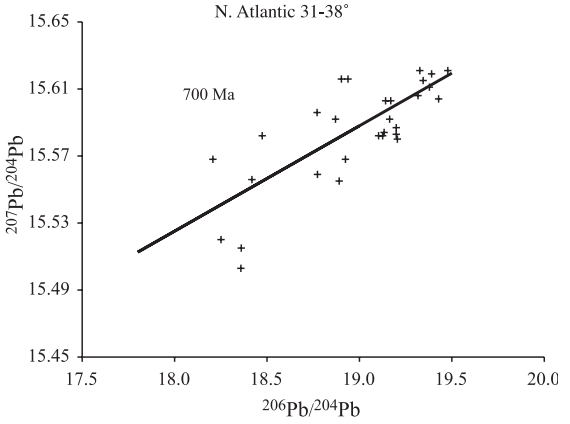

Fig. 10. $^{207}Pb/^{204}Pb$–$^{206}Pb/^{204}Pb$ ages. The two-box model predicts older $^{207}Pb/^{204}Pb$–$^{206}Pb/^{204}Pb$ (Pb–Pb) ages than conventional U–Pb ages. When the ^{238}U–^{206}Pb age is ~300 Ma, the model predicts a Pb–Pb age of ~700 Ma. Pb isotope data for the North Atlantic from 31° to 38°N [48] (shown) and from the SEIR [49] are consistent with the predicted Pb–Pb age of ~700 Ma.

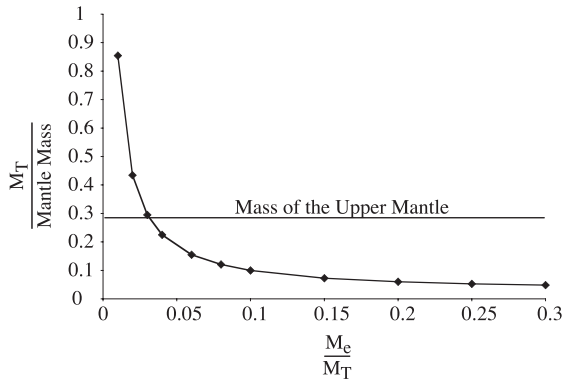

Fig. 11. Volume of mantle processed. If the mass processed in the two-box model corresponds to the melting processes at ridges, then as M_e becomes smaller the total size of the two-box system (M_T=M_e+M_d) becomes larger. M_T equals the size of the upper mantle when M_e/M_T~3.2%, the approximate frequency of E-MORB at MARK. "Mantle Mass" is the total mass of the mantle.

enriched reservoir mass (based on Eq. (10)). From the chemistry of MORB and modeling of E-MORB formation, α_D=1.4–1.8 for these elements. We can estimate M_e by considering the fraction of E-MORB to total basalts erupted at ridges. About 2% of MARK samples are E-MORB, while segments of the EPR yield as much as ~10% E-MORB [5]. If α_D=1.7, T*=0.300 Ga, and M_e=10% of the total system involved in creating the enriched reservoir (M_T=M_e+M_d), then τ_e^D=0.357 Ga (Eq. (10) and Fig. 11). The mass flux per Ga is determined by $\dot{m}=M_e/\tau_e$ and is 28% of the total system.

While $\alpha_{Nd,Sr,Pb}$ is ~1.4–1.8, more incompatible elements such as Th and Ba in E-MORB sources are a factor of 10 or more abundant than in typical N-MORB sources, requiring $\alpha_{Th,Ba}\geq 10$. This constrains the amount of depleted mantle that must be processed to create the E-MORB reservoir. A mass flux that creates a 10-fold enrichment of Th in a given volume of mantle must efficiently extract Th from 10 times that volume. For the case of M_e/M_T=0.1 and $\dot{m}$=0.28M_T/Ga, the amount of depleted mantle processed per Ga ($\dot{m}_p$) to deliver the requisite Th to the E-MORB source is 10 times greater, or $\dot{m}_p$=2.8M_T/Ga.

To understand what "processed mantle" represents, we consider that ~5 km of ocean crust is generated from ~100 km thickness of mantle. This crust contains incompatible elements extracted from >20 times its volume and is an example of how large volumes of mantle can be processed and "mined" for such elements. This cannot in itself lead to the creation of the E-MORB reservoir, however, because as shown above, the E-MORB source requires low-degree melt metasomatism of normal (N-MORB) mantle, and ocean crust is not generated by such low-degree melts. The problem of large source volumes is easily solved by the preconcentration of elements such as Ba and Th in the ocean crust, followed by low-degree melting of the recycled crust that metasomatises the peridotite mantle. Low-degree melting of subducted oceanic crust at subduction zones could effectively deliver the incompatible elements previously derived from a large volume of mantle beneath the ridge to a much smaller volume, combining the trace-element signature of low-degree partial melting with a large source volume. At a later time, high-degree melting of this metasomatised source beneath ridges generates E-MORB (Fig. 1b). In this way, it is possible during the ridge stage to process a volume as large as the ocean ridge melting regime and "preconcentrate" trace elements in oceanic crust and later to deliver these melts through low-degree melting of subducted oceanic crust to the overlying mantle wedge to form the E-MORB source and still later to melt that source to large extents under ocean ridges to form the next generation of E-MORB (Fig. 12).

If the "processed mass" is therefore the size of the ocean ridge melting regime, we can calculate the size of the total system required for generating E-MORB. If 15 km^3 of ocean crust is created per year with an average thickness of 5 km, and the mantle is processed to a depth of 100 km, then the amount of source mantle processed through ridges at current rates (i.e., $\dot{m}_p$) is approximately 3×10^{11} km^3/Ga, which is the mantle volume above 670 km. As shown above, when M_e/M_T is 10%, $\dot{m}_p$=2.8M_T/Ga, and hence, a volume equivalent to 2.8 total reservoirs must be processed per Ga to account for highly incompatible elements such as Th and Ba. To achieve this, the total size of the system (M_T) would have to be 1/2.8 or 35% of the upper mantle. As shown above, smaller M_e implies larger M_T (Fig. 11), and most ridges erupt <10% E-MORB. If M_e/M_T=0.032 (the fraction of E-MORB at MARK), and T*~0.300 Ga, then $\tau_e^D\approx 0.317$ Ga, $\dot{m}$=0.10M_T/Ga, $\dot{m}_p$=1.0M_T/Ga,

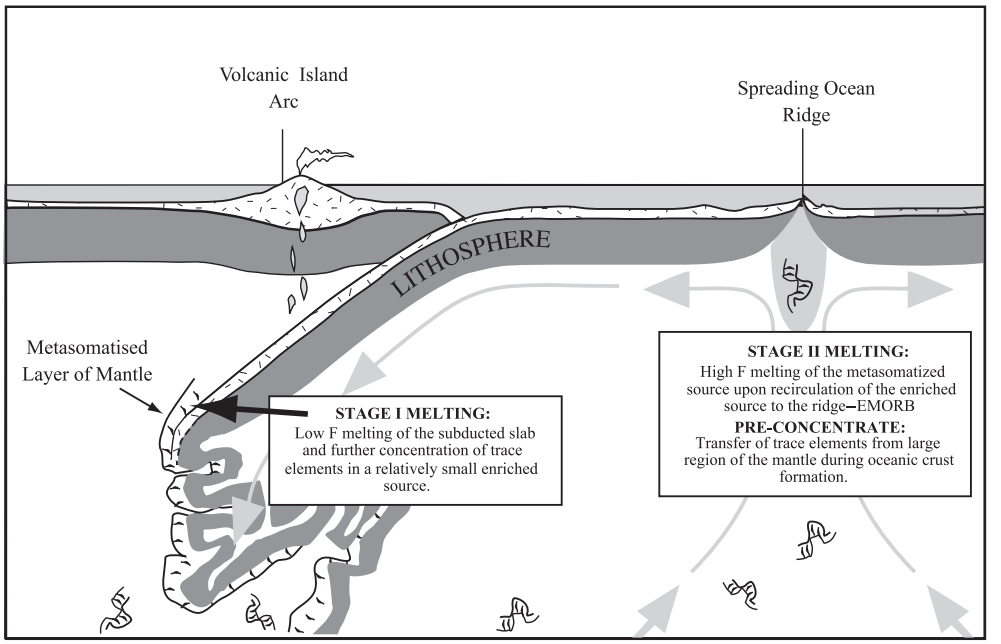

Fig. 12. Generation of E-MORB. Trace-element abundances in E-MORB require preconcentration of the highly incompatible elements from large volumes of the depleted upper mantle and two stages of melting: Stage I, low-F melting and metasomatism, and Stage II, high-F melting of the metasomatised source. These requirements are met by preconcentrating the trace elements during the formation of oceanic crust. At subduction zones, the oceanic crust partially melts to low extents and metasomatises the overlying mantle wedge. Upon recycling to the ridge by mantle convection, this metasomatised mantle melts to high extents to form E-MORB. The trace-element calculation for this model is found in Fig. 1b.

and thus M_T equals 1 upper mantle mass. Therefore, if the global occurrence of E-MORB is a few percent, then the size of the whole system is similar to that of the upper mantle.

The implication that the processes that generate E-MORB reflect convective processes in the upper mantle is also apparent from the young ages of T*. The mantle isochrons indicate a short survival time for the E-MORB reservoir, averaging only a few hundred million years between creation of enriched heterogeneities and melting at a ridge. Such time scales indicate rapid convective stirring and efficient reprocessing of the upper mantle by plate tectonics. This conclusion is in accord with an independent statistical approach made with the dispersion of helium isotope ratios [53].

Older apparent ages associated with ocean island reservoirs indicate longer survival times at greater depths and in boundary layers outside the convecting upper mantle. Thus, E-MORB formed by plume–ridge interaction should show older mantle isochron ages. Nevertheless, the chemical similarity of non-plume-related E-MORB with ocean island basalts argues for similar processes, namely, the creation of their source by addition of low-degree partial melts, to explain their trace-element patterns.

6. Conclusions

The discovery of E-MORB in the MARK area of the Mid-Atlantic Ridge, a type locality of normal depleted ridge basalt far from any plumes, shows that enriched sources independent of hot spots are widespread in the upper mantle. The chemical systematics of the MARK suite, along with other E- and N-MORB suites around the world, provide constraints on the formation processes and mantle distribution of enriched reservoirs:

(1) Ratios of highly incompatible elements require low-degree partial melting to form E-MORB,

while major- and trace-element abundances indicate higher degree melting for the final stage. Major and trace elements can be accommodated by two stages of melting where low-degree melts are first generated to form an enriched mantle source, and later, this enriched source undergoes higher melting extents under an ocean ridge. There must be a substantial time interval between the two melting events to account for the isotopic differences between E- and N-MORB.

(2) Associated basalts from all ocean basins display positive correlations on Rb–Sr, Sm–Nd, and ^{238}U–^{206}Pb isochron plots indicating "ages" of ~300 Ma, following correction for 10–15% partial melting, whereas $^{207}Pb/^{204}Pb$–$^{206}Pb/^{204}Pb$ ages are older. These ages do not reflect discrete events but rather continuous formation and destruction of E-MORB mantle sources.

(3) A two-box model describing continuous formation and destruction of enriched mantle sources by melting and convective mixing predicts steady-state "mantle isochron" ages that depend on the rate that enriched mantle sources are created and destroyed, the decay constant of the radioactive decay system, and the incompatibility of the daughter element during melting. The model predicts that Rb–Sr, Sm–Nd, and ^{238}U–^{206}Pb ages should be similar, while ^{235}U–^{207}Pb and $^{207}Pb/^{204}Pb$–$^{206}Pb/^{204}Pb$ ages are older. If creation–destruction of E-MORB sources are in steady state, the mantle isochron ages will remain constant through time. The model illuminates the simple relationships between mantle isochron ages and the residence time of the E-MORB mantle source. If the E-MORB source reservoir is small compared to the N-MORB source, then the mantle isochron age is nearly equal to the residence time of the E-MORB source.

(4) E-MORB show 10-fold enrichments of highly incompatible elements compared to N-MORB, despite generation by extents of melting similar to N-MORB. In order to achieve this level of enrichment, the element must be derived from a volume of normal mantle at least 10 times larger than the mixed source that gives rise to E-MORB. If the enrichment step takes place at depth in subduction zones, this volume constraint is easily accommodated. The incompatible trace elements are first concentrated in the oceanic crust at ocean ridges, and subsequent low-degree melting of subducted oceanic crust at subduction zones forms the enriched reservoir by metasomatising the mantle wedge. Small regions of the mantle wedge thus receive their trace-element budget from large volumes of depleted mantle. The enriched source isotopically "ages" and through mantle convection undergoes normal high extents of re-melting at the ridge.

Thus, plate tectonic processes continuously generate the enriched and depleted upper mantle reservoirs observed at ocean ridges. The mantle isochrons indicate that the average survival time of E-MORB mantle sources is ~300 Ma. If the mass of the E-MORB source reservoir is a few percent of N-MORB mantle, then the mass of the system that experiences these processes and continually feeds ocean ridge magmatism approximates that of the upper mantle.

Acknowledgements

We thank Claude Allègre, Tim Elliott, and Al Hofmann for reviews that led to improvements in the manuscript. This project was funded largely by grants from the NSF to C. Langmuir at LDEO. KED acknowledges additional support from the Lamont-Doherty Earth Observatory, and SLG's startup funds. Major contributions were made by Dana Desonie, Michael Thatcher, Cindy Van Dover, and the Captain and crew of the R/V *Atlantis II* Leg 129-7 during sample collection at sea. Cartoon illustration is by Patty Catanzaro. This is LDEO Publication 6648.

Appendix A. Supplementary data

Supplementary data associated with this article can be found, in the online version, at doi:10.1016/j.epsl.2004.07.019.

References

[1] J.G. Schilling, Iceland mantle plume: geochemical study of the Reykjanes Ridge, Nature 242 (1973) 565–571.

[2] J.-G. Schilling, M. Zajac, R. Evans, T. Johnston, W. White, J.D. Devine, R. Kingsley, Petrological and geochemcal variations along the Mid-Atlantic ridge from 29°N to 73°N, Am. J. Sci. 283 (1983) 510–586.

[3] G.N. Hanson, C.H. Langmuir, Modelling of major elements in mantle-melt systems using trace element approaches, Geochim. Cosmochim. Acta 42 (1978) 725–741.

[4] R. Kay, N.J. Hubbard, P.W. Gast, Chemical characteristics and origin of oceanic ridge volcanic rocks, J. Geophys. Res. 73 (8) (1970) 1585–1613.

[5] C.H. Langmuir, J.F. Bender, R. Batiza, Petrological and tectonic segmentation of the East Pacific Rise, 5°30′–14°30′ N, Nature 322 (6078) (1986) 422–429.

[6] B.L. Cousens, J.F. Allan, M.I. Leybourne, R.L. Chase, N.V. Wagoner, Mixing of magmas from enriched and depleted mantle sources in the northeast Pacific: West Valley segment, Juan de Fuca Ridge, Contrib. Mineral. Petrol. 120 (1995) 337–357.

[7] Y. Niu, K.D. Collerson, R. Batiza, Origin of enriched-type mid-ocean ridge basalt at ridges far from mantle plumes: the East Pacific Rise at 11°20′ N, J. Geophys. Res. 104 (1999) 7067–7087.

[8] R. Batiza, D.A. Vanko, Petrology of young Pacific seamounts, J. Geophys. Res. 89 (B13) (1984) 11,235–11,260.

[9] A. Zindler, H. Staudigel, R. Batiza, Isotope and trace element geochemistry of young Pacific seamounts: implications for the scale of upper mantle heterogeneity, Earth Planet. Sci. Lett. 70 (1984) 175–195.

[10] Y.L. Niu, R. Batiza, Trace element evidence from seamounts for recycled oceanic crust in the Eastern Pacific mantle, Earth Planet. Sci. Lett. 148 (1997) 471–483.

[11] C.J. Allègre, B. Hamelin, B. Dupré, Statistical analysis of isotopic ratios in MORB: the mantle blob cluster model and the convective regime of the mantle, Earth Planet. Sci. Lett. 71 (1984) 71–84.

[12] A. Zindler, S.R. Hart, Chemical Geodynamics. Mantle chemical heterogeneity: a matter of scale, Ann. Rev. Earth Planet. Sci. 14 (1986) 493–571.

[13] C.C. Lundstrom, J. Gill, Q. Williams, M.R. Perfit, Mantle melting and basalt extraction by equilibrium porous flow, Science 270 (1995) 1958–1961.

[14] M.M. Hirschmann, E.M. Stolper, A possible role for garnet pyroxenite in the origin of the "garnet signature" in MORB, Contrib. Mineral. Petrol. 124 (1996) 185–208.

[15] J. Phipps Morgan, W.J. Morgan, Two-stage melting and the geochemical evolution of the mantle: a recipe for mantle plum-pudding, Earth Planet. Sci. Lett. 170 (1999) 215–239.

[16] A.W. Hofmann, W.M. White, Mantle plumes from ancient oceanic crust, Earth Planet. Sci. Lett. 57 (1982) 421–436.

[17] C.J. Allègre, D.L. Turcotte, Implications of a two-component marble-cake mantle, Nature 323 (11) (1986) 123–127.

[18] A.N. Halliday, D.C. Lee, S. Tommasini, G.R. Davies, C.R. Paslick, J.G. Fitton, D.E. James, Incompatible trace elements in OIB and MORB and source enrichments in the sub-oceanic mantle, Earth Planet. Sci. Lett. 133 (1995) 379–395.

[19] D.P. McKenzie, R.K. O'Nions, The source regions of ocean island basalts, J. Petrol. 36 (1995) 133–159.

[20] W.G. Melson, G. Thompson, T.H. Van Andel, Volcanism and metamorphism in the Mid-Atlantic ridge, 22°N Latitude, J. Geophys. Res. 73 (18) (1968) 5925–5941.

[21] W.B. Bryan, G. Thompson, J.N. Ludden, Compositional variation in normal MORB from 22°–25°N: Mid-Atlantic Ridge and Kane Fracture Zone, J. Geophys. Res. 86 (B12) (1981) 11,815–11,836.

[22] J.M. Rhodes, D.P. Blanchard, M.A. Dungan, K.V. Rodgers, J.C. Brannon, Chemistry of Leg 45 basalts, in: W.G. Melson, P.D. Rabinowitz, et al., (Eds.), Initial Reports of the Deep Sea Drilling Project, vol. 45, U.S. Government Printing Office, Washington, DC, 1978, pp. 507–512.

[23] J.R. Reynolds, C.H. Langmuir, Petrological systematics of the Mid-Atlantic Ridge south of Kane: implications for ocean crust formation., J. Geophys. Res. 102 (B7) (1997) 14,915–14,946.

[24] P.J. Michael, D.W. Forsyth, D.K. Blackman, P.J. Fox, B.B. Hanan, A.J. Harding, K.C. Macdonald, G.A. Neumann, J.A. Orcutt, M. Tolstoy, C.M. Weiland, Mantle control of a dynamically evolving spreading center: Mid-Atlantic Ridge 31–34°S, Earth Planet. Sci. Lett. 121 (1994) 451–468.

[25] L. Dosso, H. Bougault, J.L. Joron, Geochemical morphology of the North Mid-Atlantic Ridge, 10°–24°N: trace element–isotope complementarity, Earth Planet. Sci. Lett. 120 (1993) 443–462.

[26] R. Mühe, H. Bohrmann, D. Garbe-Schönberg, H. Kassens, E-MORB glasses from the Gakkel Ridge (Arctic Ocean) at 87°N: evidence for the Earth's most northerly volcanic activity, Earth Planet. Sci. Lett. 152 (1997) 1–9.

[27] A.W. Hofmann, Mantle geochemistry: the message from oceanic volcanism, Nature 385 (1997) 219–229.

[28] M.M. Hirschman, E.M. Stolper, A possible role for garnet pyroxenite in the origin of the "garnet signature" in MORB, Contrib. Mineral. Petrol. 124 (1996) 185–208.

[29] J.M. Brenan, H.F. Shaw, F.J. Ryerson, D.L. Phinney, Mineral-aqueous fluid partitioning of trace elements at 900 °C and 2.0 GPa: constraints on the trace element chemsitry of mantle and deep crustal fluids, Geochim. Cosmochim. Acta 59 (16) (1995) 3331–3350.

[30] P.J. Michael, R.L. Chase, The influence of primary magma compositions, H_2O and pressure on Mid-Ocean Ridge basalt differentiation, Contrib. Mineral. Petrol. 96 (1987) 245–263.

[31] P.D. Asimow, C.H. Langmuir, The importance of water to oceanic mantle melting regimes, Nature 421 (2003) 815–820.

[32] K.E. Donnelly, The genesis of E-MORB: extension and limitations of the hot spot model, PhD, Columbia University, 2002.

[33] C.H. Langmuir, G.N. Hanson, Calculating mineral-melt equilibria with stoichiometry, mass balance, and single component distribution coefficients, in: R.C. Newton, A. Navrotsky, B.J. Wood (Eds.), Thermodynamics of Minerals

and Melts Advanced in Physical Chemistry, vol. 1, Springer-Verlag, New York, 1981, pp. 247–271.
[34] E.M. Klein, C.H. Langmuir, Global correlations of ocean ridge basalt chemistry with axial depth and crustal thickness, J. Geophys. Res. 92 (B8) (1987) 8089–8115.
[35] D.P. McKenzie, Some remarks on the movement of small melt fractions in the mantle, Earth Planet. Sci. Lett. 95 (1989) 53–72.
[36] R.K. O'Nions, D.P. McKenzie, Melting and continent generation, Earth Planet. Sci. Lett. 90 (1988) 449–4456.
[37] S.J.G. Galer, R.K. O'Nions, Magmagenesis and the mapping of chemical and isotopic variations in the mantle, Chem. Geol. 56 (1986) 45–61.
[38] T. Plank, C.H. Langmuir, Effects of the melting regime on the composition of the oceanic crust, J. Geophys. Res. 97 (B13) (1992) 19,749–19,770.
[39] D.W. Graham, A. Zindler, M.D. Kurz, W.J. Jenkins, R. Batiza, H. Staudigel, He, Pb, Sr and Nd isotope constraints on magma genesis and mantle heterogeneity beneath young Pacific seamounts, Contrib. Mineral. Petrol. 99 (1988) 446–463.
[40] C.H. Langmuir, Y.J. Su, K.E. Donnelly, S.L. Goldstein, Constraints on the mean composition and mantle source of MORB, EOS 80 (1999) 32.
[41] Y. Niu, M. Regelous, I.J. Wendt, R. Batiza, M.J. O'Hara, Geochemistry of near-EPR seamounts: importance of source vs. process and the origin of the enriched mantle component, Earth Planet. Sci. Lett. 199 (2002) 327–345.
[42] Y. Niu, M.J. O'Hara, Origin of ocean island basalts: a new perspective from petrology, geochemistry, and mineral physics considerations, J. Geophys. Res. 108 (2003) 1–19.
[43] K.E. Donnelly, C.H. Langmuir, S.L. Goldstein, Constraints on the generation of enriched mid-ocean ridge basalts, EOS 81 (2000) 1281.
[44] M. Tatsumoto, Genetic relations of oceanic basalts as indicated by lead isotopes, Science 153 (1966) 1094–1101.
[45] S.S. Sun, G.N. Hanson, Evolution of the mantle: geochemical evidence from alkali basalt, Geology 6 (1975) 297–302.
[46] C. Brooks, S.R. Hart, A. Hofmann, D.E. James, Rb–Sr mantle isochrons from oceanic regions, Earth Planet. Sci. Lett. 32 (1976) 51–61.
[47] W.M. White, J.G. Schilling, The nature and origin of geochemical variation in Mid-Atlantic Ridge basalts from central North Atlantic, Geochim. Cosmochim. Acta 42 (1978) 1501–1516.
[48] L. Dosso, H. Bougault, C.H. Langmuir, C. Bollinger, O. Bonnier, J. Etoubleau, The age and distribution of mantle heterogeneity along the Mid-Atlantic Ridge (31–41°N), Earth Planet. Sci. Lett. 170 (1999) 269–286.
[49] J.J. Mahoney, D.W. Graham, D.M. Christie, K.T.M. Johnson, L.S. Hall, D.L. Vonderhaar, Between a hot spot and a cold spot: isotopic variation in the Southeast Indian Ridge asthenosphere, 86°E–118°E, J. Petrol. 43 (2002) 1155–1176.
[50] Y. Niu, R. Hekinian, Basaltic liquids and harzburgitic residues in the Garrett Transform: a case study at fast-spreading ridges, Earth Planet. Sci. Lett. 146 (1997) 243–258.
[51] A.W. Hofmann, K.P. Jochum, M. Seufert, W.M. White, Nb and Pb in oceanic basalts: new constraints on mantle evolution, Earth Planet. Sci. Lett. 79 (1986) 33–45.
[52] K.W.W. Sims, D.J. DePaolo, Inferences about mantle magma sources from incompatible element concentration ratios in oceanic basalts, Geochim. Cosmochim. Acta 61 (1997) 765–784.
[53] C.J. Allègre, E. Lewin, Isotopic systems and stirring times of the earth's mantle, Earth Planet. Sci. Lett. 136 (1995) 629–646.
[54] F. Albarède, Radiogenic ingrowth in systems with multiple reservoirs: applications to the differentiation of the mantle–crust system, Earth Planet. Sci. Lett. 189 (2001) 2001.
[55] S.-S. Sun, W.F. McDonough, Chemical and isotopic systematics of oceanic basalts: implications for mantle composition and processes, in: A.D. Saunders, M.J. Norry (Eds.), Magmatism in the Ocean Basins, Geol. Soc. London Spec. Publ. 42 (1989) 313–345.
[56] C. Allègre, O. Brevart, B. Dupré, J.F. Minster, Isotopic and chemical effects produced in a continuously differentiating convecting Earth mantle, Philos. Trans. R. Soc. London 297 (1431) (1980) 447–477.
[57] U.R. Christensen, A.W. Hofmann, Segregation of subducted oceanic crust in the convecting mantle, J. Geophys. Res. 99 (1994) 19,867–19,884.
[58] W.F. McDonough, S.S. Sun, The composition of the Earth, Chem. Geol. 120 (1995) 223–253.
[59] Y.-J. Su, Database applications to the petrogenesis of ocean ridge basalts, PhD, Columbia University, 2002.
[60] W. Todt, R.A. Cliff, A. Hanser, A.W. Hofmann, Evaluation of a ^{202}Pb–^{205}Pb double spike for high-precision lead isotope analysis, in: A. Basu, S.R. Hart (Eds.), Earth Processes: Reading the Isotopic Code, Am. Geophys. Union Geophys. Monogr. 95 (1996) 429–437.
[61] K.T.M. Johnson, Experimental cpx/and garnet/melt partitioning of REE and other trace elements at high pressures: petrogenetic implications, Mineral. Mag. 58A (1994) 454–455.
[62] S.R. Hart, T. Dunn, Experimental CPX/Melt Partitioning of 24 trace elements, Contrib. Mineral. Petrol. 113 (1993) 1–8.
[63] J.D. Blundy, B.J. Wood, Prediction of crystal-melt partition coefficients between from elastic moduli, Nature 372 (1994) 452–454.
[64] B.J. Wood, J.D. Blundy, A predictive model for rare earth element partitioning between clinopyroxene and anhydrous silicate melt, Contrib. Mineral. Petrol. 129 (1997) 166–181.
[65] V.J.M. Salters, J. Longhi, Trace element partitioning during the initial stages of melting beneath mid-ocean ridges, Earth Planet. Sci. Lett. 166 (1999) 15–30.
[66] P. Beattie, U–Th disequilibria and partitioning on melting of garnet peridotite, Nature 363 (1993) 63–65.
[67] P.B. Kelemen, N. Shimizu, T. Dunn, Relative Depletion of niobium in some arc magmas and the continental crust: partitioning of K, Nb, La, and Ce during melt/rock reaction in the upper mantle, Earth Planet. Sci. Lett. 120 (1993) 111–134.
[68] A.K. Kennedy, G.E. Lofgren, G.J. Wasserburg, An experimental study of trace element partitioning between olivine, orthopyroxene and melt in chondrules-equilibrium value and kinetic effects, Earth Planet. Sci. Lett. 115 (1993) 177–195.
[69] G.N. Hanson, Rare earth elements in petrogenetic studies of igneous systems, AREPS 8 (1980) 371–406.